

Single crystal growth and electronic structure of Rh-doped $Sr_3Ir_2O_7$

Bingqian Wang(王冰倩), Shuting Peng(彭舒婷), Zhipeng Ou(欧志鹏), Yuchen Wang(王宇晨), Muhammad Waqas, Yang Luo(罗洋), Zhiyuan Wei(魏志远), Linwei Huai(淮琳崴),Jianchang Shen(沈建昌), Yu Miao(缪宇), Xiupeng Sun(孙秀鹏), Yuewei Yin(殷月伟), and Junfeng He(何俊峰)

Citation: Chin. Phys. B, 2023, 32 (**8**): 087108. DOI: 10.1088/1674-1056/acd7d5
Journal homepage: http://cpb.iphy.ac.cn; http://iopscience.iop.org/cpb

What follows is a list of articles you may be interested in

Single crystal growth, structural and transport properties of bad metal $RhSb_2$

D S Wu(吴德胜), Y T Qian(钱玉婷), Z Y Liu(刘子懿), W Wu(吴伟), Y J Li(李延杰), S H Na(那世航), Y T Shao(邵钰婷), P Zheng(郑萍), G Li(李岗), J G Cheng(程金光), H M Weng(翁红明), J L Luo(雒建林)

Chin. Phys. B, 2020, 29 (**3**): 037101. DOI: 10.1088/1674-1056/ab696e

Benchmarking the simplest slave-particle theory with Hubbard dimer

Wei-Wei Yang(杨薇薇), Hong-Gang Luo(罗洪刚), Yin Zhong(钟寅)

Chin. Phys. B, 2019, 28 (**10**): 107103. DOI: 10.1088/1674-1056/ab3dfe

Hubbard model on an anisotropic checkerboard lattice at finite temperatures: Magnetic and metal-insulator transitions

Hai-Di Liu(刘海迪)

Chin. Phys. B, 2019, 28 (**10**): 107102. DOI: 10.1088/1674-1056/ab4279

Structure-dependent metal—insulator transition in one-dimensional Hubbard superlattice

Zhang Liang-Liang (张亮亮), Huang Jin (黄金), Duan Cheng-Bo (段丞博), Wang Wei-Zhong (王为忠)

Chin. Phys. B, 2015, 24 (**7**): 077101. DOI: 10.1088/1674-1056/24/7/077101

Emergent reversible giant electroresistance in spacially confined $La_{0.325}Pr_{0.3}Ca_{0.375}MnO_3$ wires

Cui Li-Min (崔丽敏), Li Jie (李洁), Wang Jia (王佳), Zhang Yu (张玉), Zheng Dong-Ning (郑东宁)

Chin. Phys. B, 2014, 23 (**9**): 097103. DOI: 10.1088/1674-1056/23/9/097103

RAPID COMMUNICATION

Single crystal growth and electronic structure of Rh-doped $Sr_3Ir_2O_7$

Bingqian Wang(王冰倩), Shuting Peng(彭舒婷), Zhipeng Ou(欧志鹏), Yuchen Wang(王宇晨), Muhammad Waqas, Yang Luo(罗洋), Zhiyuan Wei(魏志远), Linwei Huai(淮琳崴), Jianchang Shen(沈建昌), Yu Miao(缪宇), Xiupeng Sun(孙秀鹏), Yuewei Yin(殷月伟), and Junfeng He(何俊峰)[†]

Department of Physics and CAS Key Laboratory of Strongly-coupled Quantum Matter Physics, University of Science and Technology of China, Hefei 230026, *China*

(Received 15 April 2023; revised manuscript received 15 May 2023; accepted manuscript online 23 May 2023)

Ruddlesden-Popper iridate $Sr_3Ir_2O_7$ is a spin–orbit coupled Mott insulator. Hole doped $Sr_3Ir_2O_7$ provides an ideal platform to study the exotic quantum phenomena that occur near the metal–insulator transition (MIT) region. Rh substitution of Ir is an effective method to induce hole doping into $Sr_3Ir_2O_7$. However, the highest doping level reported in $Sr_3(Ir_{1-x}Rh_x)_2O_7$ single crystals was only around 3%, which is far from the MIT region. In this paper, we report the successful growth of single crystals of $Sr_3(Ir_{1-x}Rh_x)_2O_7$ with a doping level of $\sim 9\%$. The samples have been fully characterized, demonstrating the high quality of the single crystals. Transport measurements have been carried out, confirming the tendency of MIT in these samples. The electronic structure has also been examined by angle-resolved photoemission spectroscopy (ARPES) measurements. Our results establish a platform to investigate the heavily hole doped $Sr_3Ir_2O_7$ compound, which also provide new insights into the MIT with hole doping in this material system.

Keywords: hole doped iridate, single crystal growth, metal–insulator transition, angle-resolved photoemission spectroscopy (ARPES)

PACS: 71.10.Hf, 71.20.–b, 71.30.+h, 71.27.+a **DOI:** 10.1088/1674-1056/acd7d5

The metal–insulator transition (MIT) is a crucial phenomenon in strongly correlated material systems.[1] In the MIT region, electrons display both localized and itinerant characteristics. Interactions are expected among multiple degrees of freedom, including charge, spin, orbit, and lattice. The energy scales of these interactions are comparable, leading to the emergence of exotic physical phenomena, such as high-temperature superconductivity[2,3] and density wave orders.[4–6]

Ruddlesden-Popper strontium iridates $Sr_{n+1}Ir_nO_{3n+1}$ ($n = 1, 2$) are the so-called spin–orbit coupled Mott insulators with a perovskite crystal structure.[7–9] As a 5d-electron counterpart of the cuprate high temperature superconductors,[10] these materials have attracted much attention. Antiferromagnetic order,[11] crystal field interaction, spin–orbit coupling[12] and Coulomb interaction[13] coexist and cooperate in this material system. The double-layer compound $Sr_3Ir_2O_7$ is an ideal system to investigate the MIT as a function of doping, due to a larger bandwidth and a smaller Mott gap compared to those in Sr_2IrO_4 (the single-layer compound).[14,15]

In recent years, the electronic structure of the $Sr_3Ir_2O_7$ system has been investigated as a function of the carrier doping.[16–25] On the electron doped side, La substitution of Sr has been applied. Earlier studies have proposed multiple similarities between the La-doped $Sr_3Ir_2O_7$ and cuprates. For example, an anomalous effective mass enhancement has been reported in La-doped $Sr_3Ir_2O_7$,[19] which is similar to that in the cuprates. Nevertheless, other studies indicate a conventional, weakly correlated Fermi liquid state in La-doped $Sr_3Ir_2O_7$, different from that in cuprates.[17]

In order to achieve a complete understanding of the doped $Sr_3Ir_2O_7$, the hole doped side should also be systematically investigated. There are primarily two ways to introduce holes, the substitution of Ir by either Ru or Rh.[20–25] For Ru substitution, a significant amount of Ru (35%–40%) is required to reach the MIT region.[22–24] In this regard, it has been debated whether (or to what extent) such samples can still represent the properties of iridates. Compared to Ru, the Rh substitution is more efficient in doping holes into the $Sr_3Ir_2O_7$ compound. It has been suggested that the average energy of the t_{2g} states of Rh and Ir is similar, but the band splitting effect in Ir is larger due to a larger spin–orbit coupling. Therefore, $J_{1/2}$ electrons from neighboring Ir atoms will fill the $J_{1/2}$ state at the Rh site, leaving a hole at the Ir site.[26] However, for the $Sr_3(Ir_{1-x}Rh_x)_2O_7$ single crystals, the highest doping level achieved so far is only $\sim 3\%$.[20] This is still far away from the MIT region.

In this paper, we report the successful growth of high-quality single crystals of $Sr_3(Ir_{1-x}Rh_x)_2O_7$ with a doping level of $\sim 9\%$, which exhibit a clear trend towards the MIT. Energy dispersive x-ray spectroscopy (EDX) measurements confirm the successful Rh substitution. X-ray diffraction (XRD)

[†]Corresponding author. E-mail: jfhe@ustc.edu.cn

© 2023 Chinese Physical Society and IOP Publishing Ltd

measurements reveal the high quality of the crystals. Resistivity measurements and angle-resolved photoemission spectroscopy (ARPES) unveil the trend towards the MIT. This material provides an ideal platform to study the exotic quantum phenomena associated with the MIT in hole doped spin–orbit coupled Mott insulators.

High-quality single crystals of $Sr_3(Ir_{0.91}Rh_{0.09})_2O_7$ were grown in platinum crucibles using IrO_2 (99.99%, Alfa Aesar), RhO_2 (Rh 75.2%–77.4%, Alfa Aesar), $SrCO_3$ (99.99%, Alfa Aesar) and $SrCl_2$ (99.5%, Alfa Aesar) in a 1.8:0.2:3:15 molar ratio. The flux method was used to grow the doped samples, similar to that used for the growth of parent compound.[27,28] All the powders were dried initially to minimize the presence of moisture during the reaction. The powders were then weighted and mixed in an agate mortar, and ground for 1.5 h. Then, the mixture was moved into a platinum crucible with a Pt lid, which was further contained inside an alumina crucible. We note that the Rh-doped $Sr_3Ir_2O_7$ bilayer structure is not very stable, and it is difficult to grow high quality single crystals with a high Rh doping level. Therefore, a systematic optimization of the growth conditions has been carried out, which revealed the importance of growth temperature and cooling rate for the successful growth of Rh-doped $Sr_3Ir_2O_7$. The mixture was heated to 1270 °C, followed by a cooling process during which the temperature was decreased to 800 °C at a rate of 7.8 °C/h. The mixture was then furnace-cooled to 400 °C, and finally cooled naturally to the room temperature. In this way, we have successfully obtained single crystals with the Rh doping level of 8%–10%, which is beyond the highest doping level reported before. Compared to the growth conditions in the earlier studies, our growth temperature is higher and the cooling rate is smaller.[20] The single crystals of $Sr_3(Ir_{0.91}Rh_{0.09})_2O_7$ exhibit a tetragonal shape, with a flat surface. These plate-like samples have typical dimensions of $\sim 1.5 \times 1.5 \times 0.1$ mm^3 (as shown in Fig. 1(c)).

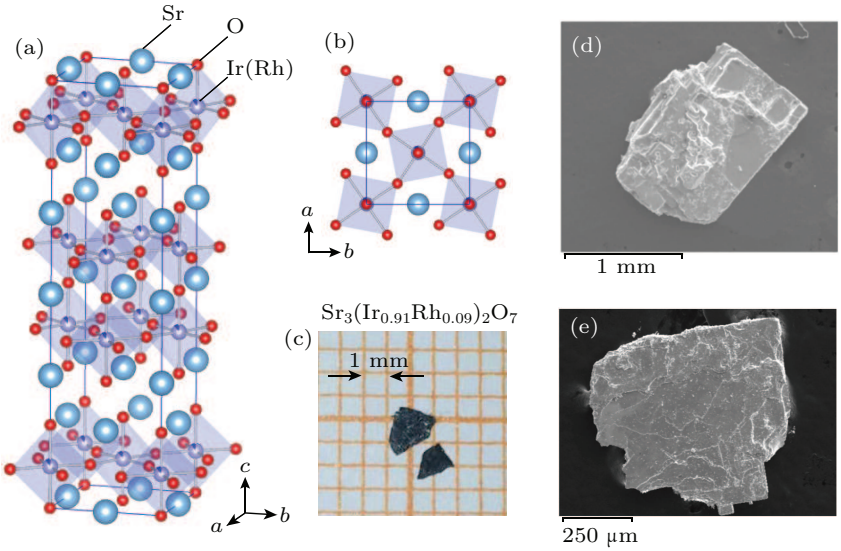


Fig. 1. (a) Crystal structure of $Sr_3(Ir_{0.91}Rh_{0.09})_2O_7$. (b) The IrO_6 octahedral rotation in $Sr_3(Ir_{0.91}Rh_{0.09})_2O_7$. (c) Image of the as-grown $Sr_3(Ir_{0.91}Rh_{0.09})_2O_7$ single crystals. (d) and (e) The surface morphology of the $Sr_3(Ir_{0.91}Rh_{0.09})_2O_7$ single crystals observed by SEM.

Figure 1(a) shows the crystal structure of $Sr_3(Ir_{0.91}Rh_{0.09})_2O_7$, where the substitution of Ir atoms by Rh atoms is highlighted. Figure 1(b) reveals the octahedral rotation in the $Sr_3(Ir_{0.91}Rh_{0.09})_2O_7$ compound. This lattice distortion is a critical feature of the crystal structure and plays a fundamental role in determining the material's properties. Surface topography and chemical composition of the $Sr_3(Ir_{1-x}Rh_x)_2O_7$ crystals have been obtained with the aid of a scanning electron microscope (SEM) equipped with energy dispersive x-ray spectroscopy (EDX). Figures 1(d) and 1(e) are the SEM images of the doped samples. The EDX results of the sample in Fig. 1(d) are shown in Table 1. The average atomic ratio of Sr:Ir is very close to 3:2, and the Rh concentration is about 9%. The samples with other doping levels have been characterized in the similar way. The highest doping level we can achieve is around 10%.

Table 1. SEM/EDX results on the as-grown single crystal.

Element	Weight (%)	Atomic (%)
Sr	31.29	21.2
Ir	45.25	14.2
Rh	2.87	1.4

The x-ray diffraction (XRD) results of the as-grown $Sr_3(Ir_{1-x}Rh_x)_2O_7$ crystal are presented in Fig. 2. The peaks of the doped sample (Fig. 2(a)) correspond to the (0, 0, n) reflections of the $Sr_3Ir_2O_7$ lattice structure, indicating that the substitution of Ir atoms by Rh atoms does not significantly change the overall crystal structure of the $Sr_3Ir_2O_7$ lattice. Figure 2(b) shows the single crystal rocking curve, which exhibits only one sharp peak with a full width at half maxima (FWHM) of

0.1°. The sharpness of the peak reflects the quality of the crystal. The narrow peak and small FWHM in our measurements indicate the high quality of the as-grown $Sr_3(Ir_{0.91}Rh_{0.09})_2O_7$ sample. The XRD results also rule out any possible contamination from the Sr_2IrO_4 phase. Besides, the lattice constants of the samples have been examined by the Super Nova four-circle single crystal x-ray diffractometer. The measured lattice constants of the $Sr_3Ir_2O_7$ parent compound ($a = 5.5213$ Å, $b = 5.5238$ Å, $c = 20.947$ Å) are consistent with the previous report within the experimental error bar. The corresponding lattice volume is 638.86 Å^3. For the 9% Rh-doped sample, the lattice constants are $a = 5.5124$ Å, $b = 5.5180$ Å, $c = 20.898$ Å, and the lattice volume is 635.66 Å^3. The slight changes are reasonable since the Rh atoms are smaller than the Ir atoms. The successfully grown heavily Rh doped $Sr_3(Ir_{1-x}Rh_x)_2O_7$ single crystals provide a unique platform to investigate the associated physical properties.

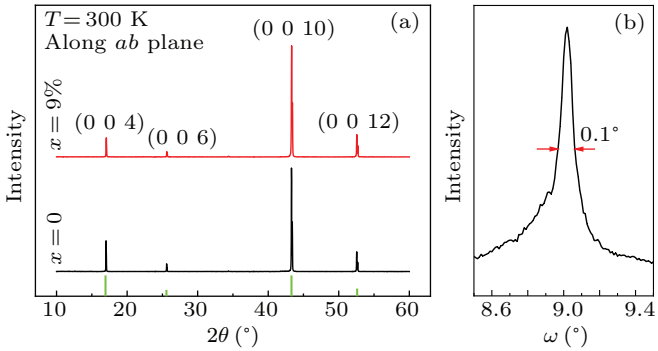


Fig. 2. (a) XRD patterns of the $Sr_3(Ir_{0.91}Rh_{0.09})_2O_7$ single crystal (red), $Sr_3Ir_2O_7$ single crystal (black) and the calculated peak positions of $Sr_3Ir_2O_7$ (green). All peaks of the $Sr_3(Ir_{0.91}Rh_{0.09})_2O_7$ can be indexed by (0, 0, n) of the $Sr_3Ir_2O_7$ lattice structure. (b) The rocking curve of the $Sr_3(Ir_{0.91}Rh_{0.09})_2O_7$ single crystal.

After fully characterizing the samples, we next investigate the physical properties by electrical measurements. Figure 3(a) compares the resistivity–temperature (R–T) curves of $Sr_3(Ir_{1-x}Rh_x)_2O_7$ samples with different doping levels. The R–T curve of the parent compound ($x = 0$) is similar to a typical one in previous results.[29,30] But significant changes can be seen in the R–T curve of the doped samples. First, the overall magnitude of the resistivity drops by several orders of magnitude in the doped samples, indicating a less insulating state. Second, the parent compound and relatively low-doping sample ($x = 6.5\%$) show an insulating behavior ($\delta\rho/\delta T < 0$) at all temperatures, whereas the high-doping samples ($x > 9\%$) exhibit a metallic-like behavior at high temperatures (although they still show a little insulating behavior in the low temperature region). We note that the metal–insulator transition temperature gradually decreases when the doping level increases.

In order to explore the electronic structure of the $Sr_3(Ir_{0.91}Rh_{0.09})_2O_7$ near MIT, we have carried out high resolution ARPES measurements at Beamline 5-2 of the Stanford Synchrotron Radiation Lightsource (SSRL) at SLAC National Accelerator Laboratory. The photon energy of 100 eV has been used for the measurements, with a total energy resolution of ~ 11 meV. The single crystals were cleaved *in situ* and measured with an ultra-high vacuum of better than 3×10^{-11} Torr at 25 K.

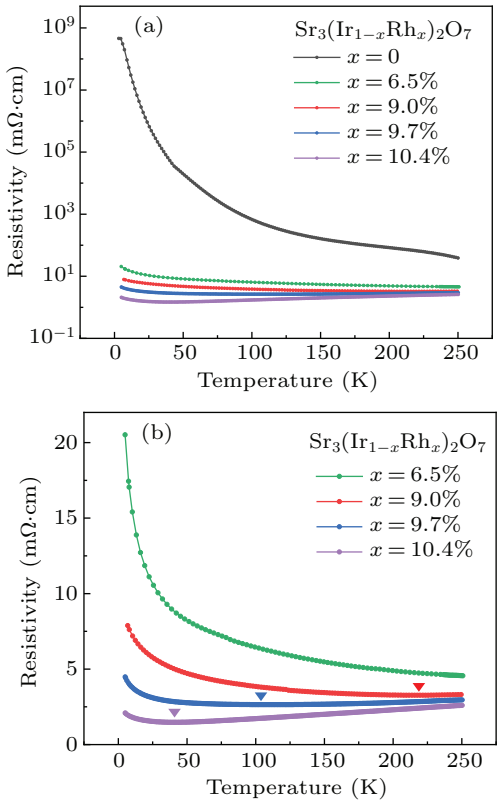


Fig. 3. (a) Temperature dependence of the *ab*-plane resistivity for $Sr_3Ir_2O_7$ with different Rh-doping levels. (b) Same as (a), but plotted in an expanded scale for the doped samples. The metal–insulator transition temperatures are marked.

Figure 4(a) shows the Fermi surface map. Rectangle-shaped spectral weight can be clearly identified around the X points, which is contributed by the top of the hole-like bands at X. In Fig. 4(b), the constant energy map at $E = -150$ meV is shown, where the spectral weight from the top of the hole-like bands at Γ can be observed. The solid (dotted) red lines in Figs. 4(a) and 4(b) represent the undistorted (distorted) Brillouin zone (BZ). The bilayer structure of $Sr_3(Ir_{0.91}Rh_{0.09})_2O_7$ gives rise to double-band features around the X and Γ points, which is different from that in the Sr_2IrO_4 system. This is highlighted in Fig. 4(d), where the second derivative image clearly reveals the double-band features around the X and Γ points. These features can also be seen in the raw data. Figures 4(e) and 4(f) show a series of momentum distribution curves (MDCs) near Γ and X, respectively. The energy and momentum ranges of the MDCs are marked by the red and yellow dotted boxes in Fig. 4(c). The double-band features can be clearly identified in the MDC plots.

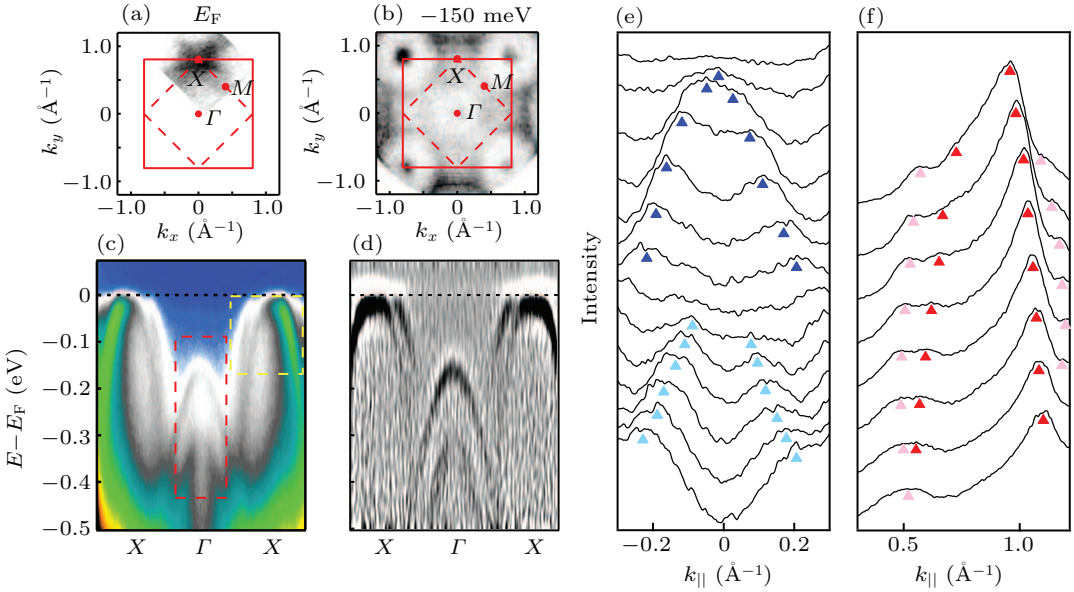


Fig. 4. (a) Fermi surface map. (b) Constant energy map at $E_b = -150$ meV. (c) ARPES spectrum measured along the ΓX direction. (d) Second derivative image of the spectrum in (c). (e) MDCs taken from the red dotted box in (c). The peaks are marked by dark blue and light blue solid triangles. (f) MDCs taken from the yellow dotted box in (c). The dark red and light red solid triangles indicate the peaks.

Most importantly, the top of the hole-like band at the X point of the $Sr_3(Ir_{0.91}Rh_{0.09})_2O_7$ sample is at the vicinity of the Fermi level (E_F), with a small gap of approximately 10–20 meV. This is distinct from that in the parent compound, where the top of the hole-like band at X is about 90 meV below E_F.[14,31–33] The upward shift of the hole-like band is consistent with hole doping in the Rh-doped sample. The existence of electron density of states near E_F [Fig. 4(c)] also echoes the more metallic behavior in the $Sr_3(Ir_{0.91}Rh_{0.09})_2O_7$ sample. In this regard, systematic temperature dependent measurements are stimulated for the future study, in order to reveal whether the metallic behavior at 250 K in the R–T measurements represents a real electronic phase transition. Nevertheless, we note that temperature dependent measurements on $Sr_{n+1}Ir_nO_{3n+1}$ ($n = 1, 2$) samples are challenging due to the surface aging effect.[34] In the regard, a local heating device might be helpful.[35]

In conclusion, we have successfully grown high quality single crystals of the spin–orbit coupled Mott insulator $Sr_3(Ir_{1-x}Rh_x)_2O_7$ using a flux method. The crystal structure has been confirmed by x-ray diffraction, and the doping levels have been verified by EDX measurements. The resistivity data reveal metal–insulator transition in samples with high Rh-doping levels. The electronic structure of the $Sr_3(Ir_{0.91}Rh_{0.09})_2O_7$ sample has been revealed by ARPES measurements. The energy shift of the electron band is consistent with hole doping. Electron density of states is observed at the vicinity of the Fermi level, echoing the metallic behavior of this material. The successful growth of heavily Rh doped $Sr_3Ir_2O_7$ single crystals provides us with a unique platform to further investigate the exotic physical properties of doped Mott insulators near the MIT region.

Acknowledgements

We thank M. Hashimoto and D. Lu for their support in ARPES measurements. We thank J. Y. Zhao, X. G. Liu, L. Chen, and Y. H. Zhao for their assistance in electrical and XRD measurements. The work at University of Science and Technology of China (USTC) was supported by the USTC start-up fund, the National Natural Science Foundation of China (Grant Nos. 12074358 and 12004363), the Fundamental Research Funds for the Central Universities (Grant Nos. WK3510000008 and WK2030000035), and the Innovation Program for Quantum Science and Technology (Grant No. 2021ZD0302802). Use of the Stanford Synchrotron Radiation Lightsource, SLAC National Accelerator Laboratory is supported by the U.S. Department of Energy, Office of Science, Office of Basic Energy Sciences under Contract No. DE-AC02-76SF00515.

References

[1] Imada M, Fujimori A and Tokura Y 1998 *Rev. Mod. Phys.* **70** 1039
[2] Dynes R C, Garno J P, Hertel G B and Orlando T P 1984 *Phys. Rev. Lett.* **53** 2437
[3] Klein T, Achatz P, Kacmarcik J, Marcenat C, Gustafsson F, Marcus J, Bustarret E, Pernot J, Omnes F, Sernelius B E, Persson C, Ferreira da Silva A and Cytermann C 2007 *Phys. Rev. B* **75** 165313
[4] García-Muñoz J L, Rodríguez-Carvajal J and Lacorre P 1992 *Europhys. Lett.* **20** 241
[5] Lee C H, Matsuhata H, Yamaguchi H, Sekine C, Kihou K, Suzuki T, Noro T and Shirotani I 2004 *Phys. Rev. B* **70** 153105
[6] Hillenius S J, Coleman R V, Fleming R M and Cava R J 1981 *Phys. Rev. B* **23** 1567
[7] Crawford M K, Subramanian M A, Harlow R L, Fernandez-Baca J A, Wang Z R and Johnston D C 1994 *Phys. Rev. B* **49** 9198
[8] Moon S J, Jin H, Kim K W, Choi W S, Lee Y S, Yu J, Cao G, Sumi A, Funakubo H, Bernhard C and Noh T W 2008 *Phys. Rev. Lett.* **101** 226402
[9] Bertinshaw J, Kim Y K, Khaliullin G and Kim B J 2019 *Annu. Rev. Condens. Matter. Phys.* **10** 315

[10] Subramanian M A, Crawford M K, Harlow R L, Ami T, Fernandez-Baca J A, Wang Z R and Johnston D C 1994 *Physica C* **235** 743

[11] Nagai I, Yoshida Y, Ikeda S I, Matsuhata H, Kito H and Kosaka M 2007 *J. Phys.: Condens. Matter* **19** 136214

[12] Rau J G, Lee E K H and Kee H Y 2016 *Annu. Rev. Condens. Matter. Phys.* **7** 195

[13] Kim B J, Jin H, Moon S J, Kim J Y, Park B G, Leem C S, Yu J, Noh T W, Kim C, Oh S J, Park J H, Durairaj V, Cao G and Rotenberg E 2008 *Phys. Rev. Lett.* **101** 076402

[14] Wang Q, Cao Y, Waugh J A, Park S R, Qi T F, Korneta O B, Cao G and Dessau D S 2013 *Phys. Rev. B* **87** 245109

[15] Carter J M and Kee H Y 2013 *Phys. Rev. B* **87** 014433

[16] He J, Hafiz H, Mion T R, Hogan T, Dhital C, Chen X, Lin Q, Hashimoto M, Lu D H, Zhang Y, Markiewicz R S, Bansil A, Wilson S D and He R H 2015 *Sci. Rep.* **5** 8533

[17] de la Torre A, Hunter E C, Subedi A, McKeown Walker S, Tamai A, Kim T K, Hoesch M, Perry R S, Georges A and Baumberger F 2014 *Phys. Rev. Lett.* **113** 256402

[18] Hogan T, Dally R, Upton M, Clancy J P, Finkelstein K, Kim Y J, Graf M J and Wilson S D 2016 *Phys. Rev. B* **94** 100401

[19] Affeldt G, Hogan T, Denlinger J D, Vishwanath A, Wilson S D and Lanzara A 2018 *Phys. Rev. B* **97** 125111

[20] Brouet V, Serrier-Garcia L, Louat A, Fruchter L, Bertran F, Le Fèvre P, Rault J, Forget A and Colson D 2018 *Phys. Rev. B* **98** 235101

[21] Song S, Kim S, Ahn G H, Seo J H, Schmehr J L, Aling M, Wilson S D, Kim Y K and Moon S J 2018 *Phys. Rev. B* **98** 035110

[22] Schmehr J L, Mion T R, Porter Z, Aling M, Cao H, Upton M H, Islam Z, He R H, Sensarma R, Trivedi N and Wilson S D 2019 *Phys. Rev. Lett.* **122** 157201

[23] Dhital C, Hogan T, Zhou W, Chen X, Ren Z, Pokharel M, Okada Y, Heine M, Tian W, Yamani Z, Opeil C, Helton J S, Lynn J W, Wang Z, Madhavan V and Wilson S D 2014 *Nat. Commun.* **5** 3377

[24] Wang Z, Okada Y, O'Neal J, Zhou W, Walkup D, Dhital C, Hogan T, Clancy P, Kim Y J, Hu Y F, Santos L H, Wilson S D, Trivedi N and Madhavan V 2018 *Proc. Natl. Acad. Sci. USA* **115** 11198

[25] Ahn G, Schmehr J L, Porter Z, Wilson S D and Moon S J 2020 *Sci. Rep.* **10** 22340

[26] Cao Y, Wang Q, Waugh J A, Reber T J, Li H, Zhou X, Parham S, Park S R, Plumb N C, Rotenberg E, Bostwick A, Denlinger J D, Qi T, Hermele M A, Cao G and Dessau D S 2016 *Nat. Commun.* **7** 11367

[27] Sung N H, Gretarsson H, Proepper D, Porras J, Le Tacon M, Boris A V, Keimer B and Kim B J 2016 *Philos. Mag.* **96** 413

[28] Manna K, Aslan-Cansever G, Maljuk A, Wurmehl S, Seiro S and Büchner B 2020 *J. Cryst. Growth* **540** 125657

[29] Dhital C, Khadka S, Yamani Z, de la Cruz C, Hogan T C, Disseler S M, Pokharel M, Lukas K C, Tian W, Opeil C P, Wang Z and Wilson S D 2012 *Phys. Rev. B* **86** 100401

[30] Fujiyama S, Ohashi K, Ohsumi H, Sugimoto K, Takayama T, Komesu T, Takata M, Arima T and Takagi H 2012 *Phys. Rev. B* **86** 174414

[31] Moreschini L, Moser S, Ebrahimi A, Dalla Piazza B, Kim K S, Boseggia S, McMorrow D F, Rønnow H M, Chang J, Prabhakaran D, Boothroyd A T, Rotenberg E, Bostwick A and Grioni M 2014 *Phys. Rev. B* **89** 201114

[32] Okada Y, Walkup D, Lin H, Dhital C, Chang T R, Khadka S, Zhou W, Jeng H T, Paranjape M, Bansil A, Wang Z, Wilson S D and Madhavan V 2013 *Nat. Mater.* **12** 707

[33] Park H J, Sohn C H, Jeong D W, Cao G, Kim K W, Moon S J, Jin H, Cho D Y and Noh T W 2014 *Phys. Rev. B* **89** 155115

[34] Liu G, Wang G, Zhu Y, Zhang H, Zhang G, Wang X, Zhou Y, Zhang W, Liu H, Zhao L, Meng J, Dong X, Chen C, Xu Z and Zhou X J 2008 *Rev. Sci. Instrum.* **79** 023105

[35] Chen S D, Hashimoto M, He Y, Song D, Xu K J, He J F, Devereaux T P, Eisaki H, Lu D H, Zaanen J and Shen Z X 2019 *Science* **366** 1099